

Semantic-aware Adversarial Fine-tuning for CLIP

Jiacheng Zhang

*School of Computing and Information Systems
The University of Melbourne*

jiacheng.zhang6@unimelb.edu.au

Jinhao Li

*School of Computing and Information Systems
The University of Melbourne*

jinhao.li2@unimelb.edu.au

Hanxun Huang

*School of Computing and Information Systems
The University of Melbourne*

curtis.huang1@unimelb.edu.au

Sarah M. Erfani

*School of Computing and Information Systems
The University of Melbourne*

sarah.erfani@unimelb.edu.au

Benjamin I.P. Rubinstein

*School of Computing and Information Systems
The University of Melbourne*

benjamin.rubinstein@unimelb.edu.au

Feng Liu

*School of Computing and Information Systems
The University of Melbourne*

feng.liu1@unimelb.edu.au

Reviewed on OpenReview: <https://openreview.net/forum?id=SzZOBzueKO>

Abstract

Recent studies have shown that CLIP model’s adversarial robustness in zero-shot classification tasks can be enhanced by adversarially fine-tuning its image encoder with *adversarial examples* (AEs), which are generated by minimizing the *cosine similarity* between images and a hand-crafted template (e.g., “A photo of a {label}”). However, it has been shown that the cosine similarity between a single image and a single hand-crafted template is insufficient to measure the similarity for image-text pairs. Building on this, in this paper, we find that the AEs generated using cosine similarity may *fail to fool* CLIP when the similarity metric is replaced with semantically enriched alternatives, making the image encoder fine-tuned with these AEs less robust. To overcome this issue, we first propose a *semantic-ensemble attack* to generate semantic-aware AEs by minimizing the average similarity between the original image and an ensemble of *refined* textual descriptions. These descriptions are initially generated by a foundation model to capture core semantic features beyond hand-crafted templates and are then refined to reduce hallucinations. To this end, we propose **Semantic-aware Adversarial Fine-Tuning** (SAFT), which fine-tunes CLIP’s image encoder with semantic-aware AEs. Extensive experiments show that SAFT outperforms current methods, achieving substantial improvements in zero-shot adversarial robustness across 16 datasets. Our code is available at: <https://github.com/tmlr-group/SAFT>.

1 Introduction

Contrastive language-image pre-training (CLIP) (Radford et al., 2021) is a widely adopted framework that learns to encode text and images into a unified feature space using large datasets. This approach

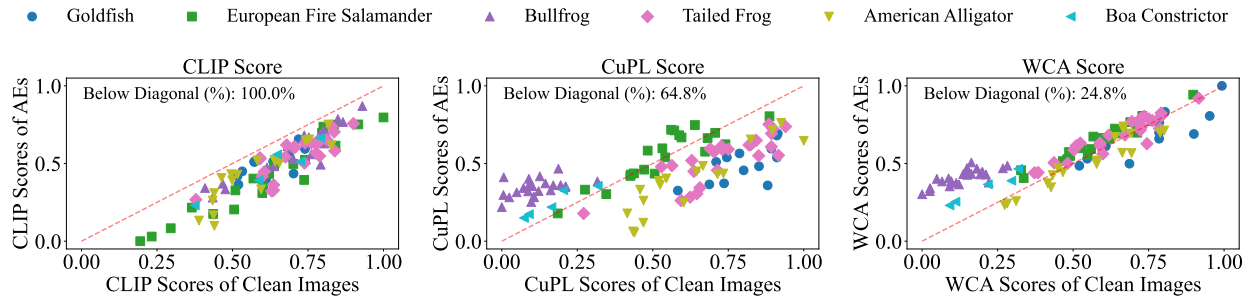


Figure 1: Comparison between CLIP (Radford et al., 2021), CuPL (Pratt et al., 2023) and WCA (Li et al., 2024) as similarity metrics for clean images and their corresponding AEs, generated by minimizing the CLIP score via *projected gradient descent* (PGD) (Madry et al., 2018), across six animal classes in ImageNet-1K (Deng et al., 2009). Points below the diagonal line indicate a success in attacking the similarity metric. The results show that although these AEs can reduce the CLIP score, they may *fail to fool* CLIP when more semantically enriched scores are used as alternatives. This observation motivates us to rethink how AEs should be constructed in the case of CLIP.

enables remarkable zero-shot generalization capabilities and has been applied across numerous downstream applications, including large *vision-language models* (VLMs) such as Flamingo (Alayrac et al., 2022) and LLaVA (Liu et al., 2023). However, despite the remarkable success of CLIP-based models across a wide range of downstream tasks, their vulnerability to *adversarial examples* (AEs) raises significant concerns about their safe deployment in real-world scenarios (Mao et al., 2023; Huang et al., 2025; Ma et al., 2025).

Fine-tuning the CLIP’s image encoder with *adversarial training* (AT) has emerged as an effective approach to enhancing its adversarial robustness (Mao et al., 2023; Schlarbmann et al., 2024; Wang et al., 2024a; Yu et al., 2024; Zhang et al., 2024). The core idea of AT is to improve model robustness by training on AEs that are generated dynamically during the training process (Madry et al., 2018). AEs are typically generated by maximizing the cross-entropy loss between the model’s predicted class probability and the true label (Goodfellow et al., 2015; Madry et al., 2018). In the case of CLIP, this probability is derived from the cosine similarity between a single image and a hand-crafted text template (e.g., “A photo of a {label}”), commonly referred to as the CLIP score (Radford et al., 2021).

Recent studies (Menon & Vondrick, 2023; Pratt et al., 2023; Li et al., 2024) have shown that the CLIP score is often insufficient to fully capture image-text alignment. To address this, they propose semantically enriched similarity metrics as advanced alternatives to the CLIP score. For example, Pratt et al. (2023) propose *customized prompts via language models* (CuPL), which measures the similarity between images and LLM-generated class-specific descriptions (e.g., “A platypus looks like a beaver with a duck’s bill” instead of “A photo of a platypus”). Li et al. (2024) further propose *weighted visual-text cross alignment* (WCA), which measures the similarity between localized image patches and CuPL-based descriptions. This naturally leads us to pose the following question:

Are adversarial examples generated by minimizing the CLIP score truly effective in degrading image-text alignment when evaluated under more semantically enriched similarity metrics?

In this paper, we find that these AEs may *fail to fool* CLIP when semantically enriched similarity metrics are used, as demonstrated by Figure 1. When CLIP score is used, 100% of points fall below the diagonal, indicating that these AEs successfully degrade the similarity. However, when the similarity metric is replaced by other alternatives such as WCA or CuPL, this degradation *diminishes significantly*: only 28.6% and 64.8% of AEs fall below the diagonal line under WCA and CuPL, respectively. More surprisingly, we observe that some AEs even achieve higher similarity scores than their clean counterparts (i.e., those above the diagonal), suggesting that CLIP becomes *more confident* in these inputs after the attack, in other words, these AEs somehow *assist* CLIP in making more confident predictions. This observation suggests that adversarial perturbations optimized by the CLIP score using a single hand-crafted template (e.g., “A photo of a label”) often *fail* to generalize to alternative text descriptions with richer attributes or contexts, and thus make the

generated AEs less effective during adversarial fine-tuning. Eventually, it leads to a less robust image encoder, as the success of AT-based methods (e.g., adversarial fine-tuning) critically depends on the effectiveness and universality of AEs (Madry et al., 2018).

To overcome this issue, we propose *Semantic-aware Adversarial Fine-Tuning* (SAFT), a new framework that aims to use more semantically enriched AEs to fine-tune the CLIP’s image encoder. We first propose a *semantic-ensemble attack* method, which generates *semantic-aware AEs* by minimizing the average similarity between the original image and an ensemble of *refined* textual descriptions. These textual descriptions are initially generated by a foundation model (e.g., a LLM or a MLLM), aiming to encapsulate diverse attributes, contexts, and synonyms related to each class label.

However, foundation models are known to suffer from hallucinations (Maynez et al., 2020). For instance, given the class “dog”, a foundation model might hallucinate that dog is a “winged mythical creature.” Therefore, to make sure these descriptions are semantically relevant and factually correct, we further propose *hallucination-aware description generation* method, which retains only top- K refined descriptions that are closely aligned with the class’s core semantics based on the relevance score. During adversarial fine-tuning, we optimize the parameters of CLIP’s image encoder to align AEs with a diverse set of textual descriptions selected through our hallucination-aware generation method. This encourages the encoder to map perturbed images into regions of the embedding space that are invariant to both visual perturbations and linguistic variations. We provide a visual illustration of SAFT in Figure 2 and an algorithmic description in Algorithm 1.

Through extensive experiments on 16 benchmark image datasets (including 1 in-domain dataset and 15 zero-shot datasets), we demonstrate the effectiveness of SAFT in Section 5. SAFT improves zero-shot robust accuracy over the current *state-of-the-art* (SOTA) methods by at least 3.85% on average, while also achieving the second-highest zero-shot clean accuracy across the 15 zero-shot datasets (see Table 1). In addition, we demonstrate that SAFT can scale to larger CLIP models (e.g., CLIP-L/14) in Table 4 and large datasets (e.g., ImageNet-1K) in Table 7, respectively. More importantly, we show that SAFT can generalize well to unseen text templates (see Table 10) and can be applied to other downstream tasks beyond classification such as the image-text retrieval task (see Table 5).

Our main contributions are: (1) we observe that the CLIP score, computed between a single image and a single handcrafted text template, is insufficient for accurately evaluating image-text similarity. Consequently, AEs generated by minimizing the CLIP score tend to be significantly less effective, leading to less robust image encoder. This is an aspect that has been largely overlooked in existing studies; (2) to address the above-mentioned limitation, we propose *Semantic-aware Adversarial Fine-Tuning* (SAFT), a novel framework that generates AEs by minimizing the average similarity between an image and an ensemble of selected textual descriptions during the CLIP fine-tuning process. To mitigate potential hallucinations caused by LLMs, we further propose a semantic filtering method to help remove descriptions that deviate significantly from the intended semantic meaning; (3) we empirically show that, compared to the existing adversarial fine-tuning methods, SAFT achieves a notable improvement in zero-shot accuracy-robustness trade-off on 16 benchmark image datasets against multiple adversarial attacks and generalizes well to unseen text templates.

2 Related Work

Adversarial Robustness. The vulnerability of deep learning models to AEs has been a long-standing challenge in the community and has been extensively studied (Szegedy et al., 2014; Goodfellow et al., 2015; Carlini & Wagner, 2017; Ilyas et al., 2019; Croce et al., 2021; Huang et al., 2021; Zhang et al., 2025; Sun et al., 2025). AEs are typically generated by introducing imperceptible perturbations to clean images, with the objective of misleading a classifier into making incorrect predictions. *Adversarial training* (AT) (Goodfellow et al., 2015; Madry et al., 2018; Zhang et al., 2019; Wang et al., 2020; Wu et al., 2020; Liu et al., 2021; Zhang et al., 2021; 2024) is widely regarded as the most effective strategy for defending against AEs, particularly due to its resilience against adaptive attacks (Athalye et al., 2018). However, AT often degrades performance on clean examples, a phenomenon known as the accuracy-robustness trade-off (Tsipras et al., 2019). Addressing this trade-off and achieving a better balance remains a key focus in AT research. AT works by generating AEs and incorporating them into the model’s training process, forcing the model to learn the underlying

distributions of AEs. However, most existing studies on AT focus on image classifiers trained with supervised learning and are known for being computationally expensive, making it challenging to scale for CLIP.

Vision-language Models. Recent advances in *vision-language models* (VLMs) have significantly improved multi-modal understanding by aligning visual and textual representations through large-scale pre-training. Radford et al. (2021) introduced CLIP, a pioneering model that employs contrastive learning on image-text pairs to enable zero-shot transfer across diverse tasks, demonstrating remarkable generalization. Pre-trained image encoders have been widely adopted in large VLMs (Alayrac et al., 2022; Awadalla et al., 2023; Wang et al., 2023; Bai et al., 2023; Liu et al., 2023; Zhu et al., 2024), which align the image encoder with LLMs in token embedding space via a bridging network or lightweight querying transformer (Li et al., 2023). The majority of large VLMs rely on CLIP as their pre-trained image encoder, primarily because it is trained with text supervision (Tong et al., 2024). While these large VLMs have achieved significant success across various tasks, their vulnerability to AEs (Mao et al., 2023; Schlarmann et al., 2024) raises critical concerns regarding their safe deployment. As a result, improving the robustness of CLIP has become an important challenge.

Adversarial Finetuning for CLIP. Fine-tuning the CLIP encoder with AT has emerged as a cost-effective approach to enhancing its adversarial robustness. TeCoA is the first method to improve the zero-shot robustness of VLMs, which fine-tunes CLIP encoders through AT (Mao et al., 2023). TeCoA uses a fixed zero-shot template with a class label to generate and train on AEs. FARE builds upon TeCoA by incorporating unsupervised objectives that maximize the distance in the embedding space to generate AEs (Schlarmann et al., 2024). PMG-AFT leverages auxiliary branches to minimize the embedding distance between outputs on AEs and clean examples in both the target and pre-trained models, mitigating adversarial overfitting (Wang et al., 2024a). TGA-ZSR introduces text-guided attention to further improve zero-shot robustness (Yu et al., 2024). Adversarial fine-tuning can also be extended to consider multimodal inputs (Zhou et al., 2024). Additionally, adversarial training can be performed from scratch during vision-language pretraining, though these approaches are computationally intensive (Gan et al., 2020; Wang et al., 2024b). In this work, our focus is adversarial fine-tuning for CLIP and we make the *first* attempt to show that enriched textual embeddings enable the generation of more generalizable AEs that are invariant to minor textual variations.

Textual Prompting in Vision-language Models. Although CLIP demonstrates strong zero-shot performance, its effectiveness on downstream tasks is highly dependent on prompt design, as highlighted by Radford et al. (2021) and Zhou et al. (2022). To mitigate this sensitivity, Menon & Vondrick (2023) and Pratt et al. (2023) propose to leverage the knowledge embedded in LLMs to automatically generate class-specific descriptions. Li et al. (2024) further propose to use localized visual prompting (e.g., random cropping) to obtain multiple patches representing local visual areas of the query image and then cross-align these local image patches with class-specific descriptions. Cai et al. (2025) propose to capture multiple common and unique features for each class by guiding foundation models to generate descriptive attributes and distinctive attributes. More recently, Sun et al. (2026) further improves existing methods (Pratt et al., 2023; Li et al., 2024) by proposing two complementary components to filter out redundant image crops using IoU overlap and remove repetitive or semantically similar textual descriptions via embedding-based cosine similarity. These semantically enriched textual descriptions have been shown effective for image-text alignment. However, to the best of our knowledge, whether such enriched textual descriptions improve the zero-shot accuracy-robustness trade-off remains underexplored.

In this work, motivated by our finding that AEs may *fail to fool* CLIP when alternative similarity metrics are used, we make the *first* attempt to show that semantically enriched textual descriptions can craft more generalizable AEs that are invariant to minor textual variations. We demonstrate that leveraging these AEs during adversarial fine-tuning further enhances the zero-shot accuracy-robustness trade-off.

3 Problem Setting and Preliminaries

3.1 Problem Setting

The *zero-shot adversarial robustness* problem, introduced by Mao et al. (2023), can be mathematically formulated as follows. Let \mathfrak{T} denote a distribution over unseen classification tasks. Each task $\mathcal{T} \sim \mathfrak{T}$ defines a label space with N classes and an associated data distribution $\mathcal{D}_{\mathcal{T}}$. An attacker, with full access to

task-specific ground-truth labels $y_{\mathcal{T}}$, crafts an AE within an ℓ_p -bounded perturbation set $\Delta = \{\delta : \|\delta\|_p \leq \epsilon\}$ by maximizing $\mathcal{L}(f^\theta(x + \delta), y_{\mathcal{T}})$. In contrast, the defender lacks access to the task identity \mathcal{T} or distribution $\mathcal{D}_{\mathcal{T}}$, and must train a model f^θ with parameters θ to minimize the expected worst-case risk over all tasks:

$$\min_{\theta} \mathbb{E}_{\mathcal{T} \sim \mathfrak{T}} \left[\mathbb{E}_{(x, y_{\mathcal{T}}) \sim \mathcal{D}_{\mathcal{T}}} \max_{\delta \in \Delta} \mathcal{L}(f^\theta(x + \delta), y_{\mathcal{T}}) \right].$$

This formulation stands in contrast to standard adversarial robustness, which is typically evaluated on a single, known task \mathcal{T}_0 .

3.2 Contrastive Language-Image Pre-training

Contrastive language-image pre-training (CLIP) (Radford et al., 2021) is a dual-encoder model consisting of an image encoder $f_{\text{img}}^\theta : \mathcal{I} \rightarrow \mathbb{R}^d$ and a text encoder $f_{\text{text}} : \mathcal{Z} \rightarrow \mathbb{R}^d$, where \mathcal{I} and \mathcal{Z} denote the input spaces of images and texts, and d is the dimension of the shared embedding space. For zero-shot classification, CLIP uses a template-based prompting strategy. Given a label set $\mathcal{Y} = \{y_1, \dots, y_N\}$, each label $y \in \mathcal{Y}$ is embedded into a textual prompt $p(y)$ (e.g., “A photo of a {label}”). At inference, given an image x , CLIP predicts its class by computing cosine similarities between the image embedding $f_{\text{img}}^\theta(x)$ and a set of text embeddings $\{f_{\text{text}}(p(y_i))\}_{i=1}^N$:

$$\hat{y} = \arg \max_{i \in \{1, \dots, N\}} \frac{f_{\text{img}}^\theta(x) \cdot f_{\text{text}}(p(y_i))}{\|f_{\text{img}}^\theta(x)\| \cdot \|f_{\text{text}}(p(y_i))\|},$$

where the numerator represents the dot product between image and text embeddings, and the denominator normalizes them using their ℓ_2 -norms.

3.3 Template-based Adversarial Fine-tuning

In this subsection, we present the learning objective of previous template-based adversarial fine-tuning methods and discuss their inherent limitations.

Learning Objective. Given an image $x \sim \mathcal{D}_{\mathcal{T}}$, its ground-truth label $y \in \{c_1, \dots, c_N\}$, and templated text prompts $p(c_i)$ (e.g., “A photo of a {label}”), the attacker crafts an AE within an ℓ_p -bounded perturbation set $\Delta = \{\delta : \|\delta\|_p \leq \epsilon\}$ by solving the following objective:

$$\delta^* = \arg \max_{\delta \in \Delta} \mathcal{L}(f_{\text{img}}^\theta(x + \delta), f_{\text{text}}(p(y))),$$

where \mathcal{L} is the cosine *dissimilarity* between image and text embeddings. In practice, this inner maximization is often approximated using *projected gradient descent* (PGD) (Madry et al., 2018), which iteratively updates the perturbation as follows:

$$\delta^{(t+1)} = \text{Proj}_{\Delta} \left(\delta^{(t)} + \alpha \cdot \text{sign} \left(\nabla_{\delta^{(t)}} \mathcal{L}(f_{\text{img}}^\theta(x + \delta^{(t)}), f_{\text{text}}(p(y))) \right) \right),$$

where $\delta^{(t)}$ is the perturbation at iteration t , α is the step size, and $\text{Proj}_{\Delta}(\cdot)$ denotes projection onto the ℓ_p -ball of radius ϵ . In contrast, the defender adversarially fine-tune f_{img}^θ to minimize the worst-case classification risk:

$$\min_{\theta} \mathbb{E}_{\mathcal{T} \sim \mathfrak{T}} \left[\mathbb{E}_{(x, y) \sim \mathcal{D}_{\mathcal{T}}} \mathcal{L}(f_{\text{img}}^\theta(x + \delta^*), f_{\text{text}}(p(y))) \right],$$

where θ refers to the parameters of CLIP’s image encoder.

Limitations. Template-based adversarial fine-tuning relies on fixed prompts (e.g., “A photo of a {label}”) to define class semantics in CLIP. While simple, this approach suffers from two main limitations: (1) AEs optimized by a single prompt often overfit to specific phrasings (e.g., “photo of a”) rather than the class itself, failing to transfer to alternative expressions like “An image of a {label}”; (2) fixed templates fail to capture the rich attributes and contexts of real-world classes. For example, AEs generated for “dog” may not generalize to prompts like “a barking animal”.

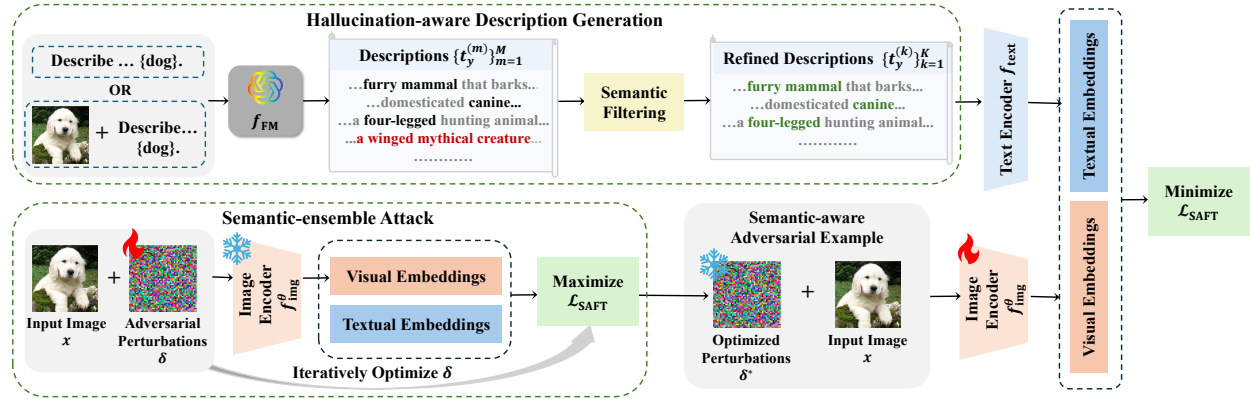


Figure 2: An overview of SAFT. In hallucination-aware description generation, a foundation model generates diverse textual descriptions for each class label, followed by the semantic filtering strategy to retain top- K most relevant descriptions. These refined descriptions are then encoded by CLIP’s text encoder. In semantic-ensemble attack, AEs are generated by maximizing misalignment between the visual embeddings and the average embeddings of refined descriptions. Finally, the image encoder is fine-tuned by minimizing this misalignment, aiming to learn linguistically invariant representations.

4 Semantic-aware Adversarial Fine-tuning

To address the limitations mentioned above, we propose a new framework called **Semantic-aware Adversarial Fine-Tuning** (SAFT), which leverages a foundation model f_{FM} (e.g., a LLM or a MLLM) to generate semantically enriched textual descriptions. Each AE is then crafted by minimizing the average similarity between the original image and the ensemble of these descriptions. In this section, we introduce key components of SAFT, which include hallucination-aware description generation, semantic-ensemble adversarial attack and the learning objective of SAFT. We provide the visual illustration in Figure 2 and the complete algorithm in Algorithm 1, respectively.

4.1 Hallucination-aware Description Generation

In this subsection, we present the hallucination-aware description generation, including the description generation method, its empirical realizations and the semantic filtering strategy.

Description Generation Method. Given a label space \mathcal{Y} , our goal is to construct a semantic mapping, where each class $y \in \mathcal{Y}$ is mapped to M textual prompts $\{t_y^{(1)}, \dots, t_y^{(M)}\}$ that capture diverse attributes, contexts, and synonyms associated with y . For instance, for the class “dog”, a foundation model might generate semantic prompts such as “a furry mammal with four legs that barks”, “a domesticated canine often kept as a pet”, or “a loyal animal trained for hunting or companionship”. These textual descriptions are generated using a foundation model f_{FM} , which we condition on class-specific instructions (e.g., “Describe the appearance of a {label}”). Formally, we define the generated descriptions \mathcal{T}_y for a class y as:

$$\mathcal{T}_y = \{t_y^{(1)}, \dots, t_y^{(M)}\} = f_{\text{FM}}(y; \phi), \quad (1)$$

where $f_{\text{FM}}(y; \phi)$ denotes the output of the foundation model conditioned on label y with generation hyperparameters ϕ (e.g., temperature for diversity). The resulting textual descriptions $\{t_y^{(m)}\}_{m=1}^M$ are subsequently encoded by CLIP’s text encoder f_{text} into M embeddings. During adversarial fine-tuning, they offer more informative training signals by encouraging the image encoder to align perturbed inputs with the entire semantic manifold of y , rather than a single text template.

Empirical Realizations. In practice, we implement two different description generation methods by adopting recent studies (Pratt et al., 2023; Cai et al., 2025):

Algorithm 1 Semantic-aware Adversarial Fine-tuning (SAFT)

Require: Pre-trained CLIP image encoder $f_{\text{img}}^\theta, f_{\text{text}}$; Class labels $\mathcal{Y} = \{y_1, \dots, y_N\}$; Generation hyperparameters ϕ ; Training epochs T ; Training dataset $\mathcal{D}_{\text{train}}$.

Ensure: Robust CLIP image encoder $f_{\text{img}}^{\theta^*}$.

```

1: for  $y \in \mathcal{Y}$  do
2:   Generate  $\{t_y^{(1)}, \dots, t_y^{(M)}\} \sim f_{\text{FM}}(y; \phi)$ 
3:   Label embedding:  $e_y \leftarrow f_{\text{text}}(y)$ 
4:   for  $m = 1$  to  $M$  do
5:     Compute  $s^{(m)}$  by Eq. (2)
6:   end for
7:   Select  $\{t_y^{(k)}\}_{k=1}^K$  by Eq. (3)
8:   Generate  $\{f_{\text{text}}(t_y^{(k)})\}_{k=1}^K$ 
9: end for
10: for epoch = 1 to  $T$  do
11:   for  $(x_j, y_j) \sim \mathcal{D}_{\text{train}}$  do
12:     Compute the optimized  $\delta_j^*$  by Eq. (4)
13:     Update  $\theta$  by Eq. (5)
14:   end for
15: end for

```

1. **SAFT-L.** This method adopts CuPL (Pratt et al., 2023), which uses a LLM to generate class-specific textual descriptions. Given a class label, the LLM is prompted with a generic query “*What does a {label} look like?*” to produce textual descriptions.
2. **SAFT-M.** This method adopts (Cai et al., 2025), which propose to capture multiple common and unique features for each class. For each class, a set of representative images is provided along with prompts like “*Describe the unique appearance of a {label} compared to other objects.*” and “*Describe the appearance of the object {label}.*” to an MLLM. The MLLM then generates descriptions that contain descriptive and distinctive attributes.

We exclude WCA (Li et al., 2024) from our realizations primarily because it requires cropping each image into multiple patches, significantly increasing computational overhead. Additionally, its text description generation is aligned with CuPL (Pratt et al., 2023). Therefore, for SAFT-L, we only adopt CuPL to generate textual descriptions.

Semantic Filtering Strategy. While foundation models can generate diverse semantic prompts for class labels, they may occasionally produce *hallucinations*: descriptions that are semantically irrelevant or factually incorrect (e.g., describing a “dog” as “a mythical creature with wings”). To address this, we introduce a *semantic filtering* strategy that retains only descriptions closely aligned with the core semantics of each class. For a given class y , we first obtain a set of M candidate prompts from the foundation model by Eq. (1), i.e., $\{t_y^{(1)}, \dots, t_y^{(M)}\} = f_{\text{FM}}(y; \phi)$. We then compute the cosine similarity between each prompt $t_y^{(m)}$ and the ground-truth label y , both encoded by CLIP’s text encoder f_{text} . The relevance score is defined as:

$$s^{(m)} = \frac{f_{\text{text}}(y) \cdot f_{\text{text}}(t_y^{(m)})}{\|f_{\text{text}}(y)\| \|f_{\text{text}}(t_y^{(m)})\|}, \quad \forall m \in \{1, \dots, M\}. \quad (2)$$

We sort the prompts by descending relevance scores:

$$\{t_y^{(m)}\} \rightarrow \text{Sort} \left(\{t_y^{(m)}\}, \{s^{(m)}\} \right), \quad \text{s.t. } s^{(1)} \geq s^{(2)} \geq \dots \geq s^{(M)}.$$

Finally, we retain the top- K most relevant prompts to define the *refined descriptions* $\tilde{\mathcal{T}}_y$:

$$\tilde{\mathcal{T}}_y = \left\{ t_y^{(k)} \right\}_{k=1}^K, \quad (3)$$

where each $t_y^{(k)}$ is among the top- K prompts ranked by $s^{(m)}$. This filtering ensures that the final descriptions consists only of prompts that are semantically faithful to the class y . For example, for the class “dog”, the foundation model may generate valid prompts like “a domesticated canine” alongside hallucinations like “a winged mythical creature.” The hallucinated prompt typically receives a low relevance score (e.g., 0.2 vs. 0.8) and is filtered out. To this end, AEs are guided by *semantically meaningful* variations, avoiding noise introduced by model hallucinations. We further conduct the ablation study in Section 5.3.

4.2 Semantic-ensemble Adversarial Attack

Building on the hallucination-aware description generation, we further propose *semantic-ensemble adversarial attack*. Unlike conventional approaches that target a single prompt, we compute perturbations that maximize the *dissimilarity* between the perturbed image embedding $f_{\text{img}}^\theta(x + \delta)$ and the full set of textual embeddings $\{f_{\text{text}}(t_y^{(1)}), \dots, f_{\text{text}}(t_y^{(M)})\}$. Formally, the optimized adversarial perturbation is obtained by solving:

$$\delta^* = \arg \max_{\delta \in \Delta} \mathcal{L}_{\text{SAFT}} \left(f_{\text{img}}^\theta(x + \delta), \{f_{\text{text}}(t_y^{(m)})\}_{m=1}^M \right), \quad (4)$$

where $\Delta = \{\delta : \|\delta\|_p \leq \epsilon\}$, and $f_{\text{FM}}(y; \phi) = \{t_y^{(m)}\}_{m=1}^M$ denotes the textual descriptions for class y generated by f_{FM} . The loss function $\mathcal{L}_{\text{SAFT}}$ measures the average cosine dissimilarity:

$$\mathcal{L}_{\text{SAFT}} \left(f_{\text{img}}^\theta(x + \delta), \{f_{\text{text}}(t_y^{(m)})\}_{m=1}^M \right) = -\frac{1}{M} \sum_{m=1}^M \frac{f_{\text{img}}^\theta(x + \delta) \cdot f_{\text{text}}(t_y^{(m)})}{\|f_{\text{img}}^\theta(x + \delta)\| \|f_{\text{text}}(t_y^{(m)})\|}.$$

This step produces stronger and more semantically enriched AEs, as it requires misalignment across multiple diverse prompts rather than a single template.

4.3 Learning Objective of SAFT

In general, SAFT formulates a bi-level optimization problem to enhance the adversarial robustness of CLIP’s image encoder. The goal is to train the encoder parameters θ such that adversarially perturbed images remain well-aligned with the diverse textual semantics produced by a foundation model f_{FM} :

$$\min_{\theta} \mathbb{E}_{(x,y)} \left[\mathcal{L}_{\text{SAFT}} \left(f_{\text{img}}^\theta(x + \delta^*), \{f_{\text{text}}(t_y^{(m)})\}_{m=1}^M \right) \right], \quad (5)$$

where δ^* is obtained by solving Eq. (4). Through this bi-level optimization, SAFT encourages the image encoder to learn representations that are robust not only to visual perturbations, but also invariant to linguistic variation across semantic prompts.

5 Experiments

5.1 Experiment Settings

Datasets. Following Yu et al. (2024), we evaluate all methods on 16 diverse datasets spanning general, fine-grained, and specialized classification tasks. These include standard benchmarks (e.g., CIFAR-10/100 (Krizhevsky et al., 2009), Tiny-ImageNet/ImageNet-1K (Deng et al., 2009), STL-10 (Coates et al., 2011), Caltech-101/256 (Griffin et al., 2007)), fine-grained datasets (e.g., Food101 (Bossard et al., 2014), Flowers102 (Nilsback & Zisserman, 2008), FGVC-Aircraft (Maji et al., 2013), StanfordCars (Krause et al., 2013), OxfordPets (Parkhi et al., 2012)), and domain-specific tasks (e.g., PCAM (Veeling et al., 2018), SUN397 (Xiao et al., 2010), EuroSAT (Helber et al., 2019) and DTD (Cimpoi et al., 2014)). Our main experiments use Tiny-ImageNet as the source dataset for adversarial fine-tuning, with the rest as unseen target tasks. We also include ImageNet-1K as an alternative source dataset in extended experiments (see Table 7 for more details).

Baselines. Following Yu et al. (2024), we compare SAFT with five representative baselines: (i) CLIP (Radford et al., 2021) fine-tuned on clean data; (ii) TeCoA (Mao et al., 2023), which applies adversarial training with fixed zero-shot prompts; (iii) FARE (Schlarmann et al., 2024), which adds unsupervised objectives to

Table 1: Clean and robust accuracy (%) against PGD-100 ($\epsilon = 1/255$) of different methods across 16 datasets. Tiny-ImageNet is the source dataset and the others are zero-shot datasets. The best accuracy is highlighted in **bold** and the second-best accuracy is underlined. “Zero-shot Average” refers to the averaged clean/robust accuracy across 15 datasets for evaluating zero-shot classification. We report standard deviations and averaged results of SAFT-L and SAFT-M for three runs.

Method	Source	Datasets for Evaluating Zero-shot Classification Accuracies																										Zero-shot Average
		CIFAR-10	CIFAR-100	CIFAR-10	CIFAR-100	Food101	STL-10	OxfordPets	Flowers102	DTD	EuroSAT	FGVC-Aircraft	Caltech-101	Caltech-256	StanfordCars	PCAM	ImageNet-1K	SUN397										
		CIFAR-10	CIFAR-100	CIFAR-10	CIFAR-100	Food101	STL-10	OxfordPets	Flowers102	DTD	EuroSAT	FGVC-Aircraft	Caltech-101	Caltech-256	StanfordCars	PCAM	ImageNet-1K	SUN397										
Robust	CLIP	13.55	19.92	4.94	0.64	40.00	2.40	0.68	2.66	0.05	0.03	14.95	9.69	0.09	1.32	1.08	0.82	6.62										
	TeCoA	31.29	31.56	16.16	14.35	65.93	34.39	19.09	16.39	10.19	1.87	52.92	40.62	8.74	45.57	15.97	16.23	26.00										
	FARE	23.88	21.25	10.72	10.97	59.59	24.56	15.48	10.96	0.14	0.84	45.96	34.35	4.38	10.17	10.54	8.30	17.88										
	PMG-AFT	32.46	<u>50.58</u>	<u>26.42</u>	16.59	68.79	35.57	15.69	12.85	9.33	1.85	53.33	36.30	5.54	48.92	15.02	16.37	27.54										
	TGA-ZSR	47.87	42.61	22.27	20.75	75.47	42.32	25.46	18.45	10.84	3.51	60.91	50.43	12.91	42.10	21.11	23.29	31.50										
	SAFT-L	53.27	52.26	28.34	<u>25.67</u>	78.97	46.07	<u>30.22</u>	20.74	12.42	4.53	64.67	54.27	15.86	47.09	22.74	26.33	35.35										
Clean	SAFT-L	(± 1.56)	(± 1.28)	(± 1.09)	(± 1.55)	(± 0.71)	(± 3.81)	(± 1.78)	(± 0.12)	(± 1.65)	(± 0.29)	(± 1.02)	(± 0.34)	(± 2.59)	(± 0.40)	(± 0.38)	(± 1.04)											
	SAFT-M	<u>50.79</u>	45.32	25.29	25.84	<u>78.48</u>	<u>43.29</u>	<u>29.48</u>	<u>19.31</u>	<u>11.95</u>	<u>4.02</u>	<u>63.36</u>	<u>53.08</u>	<u>14.40</u>	<u>46.80</u>	<u>22.43</u>	<u>23.62</u>	<u>33.78</u>										
	CLIP	79.04	84.55	54.25	47.10	93.78	80.98	46.43	30.32	24.39	9.30	78.69	70.81	31.15	47.89	44.40	46.80	52.72										
	TeCoA	54.59	66.78	34.37	33.60	85.90	61.81	34.06	24.79	18.83	6.42	70.67	60.08	22.23	52.32	31.85	34.53	43.08										
	FARE	<u>77.54</u>	87.58	62.80	70.02	<u>94.33</u>	81.47	57.10	36.33	22.69	14.19	84.04	77.50	44.35	46.07	51.78	49.91	58.68*										
	PMG-AFT	47.36	71.20	40.53	28.77	81.83	54.28	24.14	18.28	13.12	3.84	64.73	48.49	10.77	49.93	23.72	27.58	37.42										
Clean	TGA-ZSR	76.84	85.90	57.20	56.46	92.92	75.47	47.51	29.94	24.60	11.98	80.02	73.82	36.32	49.91	46.50	50.16	54.58										
	SAFT-L	73.47	85.81	57.26	58.69	93.30	77.90	48.96	30.05	<u>25.83</u>	13.39	79.89	74.39	35.18	49.86	46.61	51.91	55.27										
	SAFT-M	(± 0.41)	(± 0.84)	(± 0.91)	(± 0.47)	(± 0.33)	(± 1.15)	(± 2.97)	(± 0.28)	(± 5.42)	(± 1.09)	(± 1.31)	(± 0.25)	(± 0.64)	(± 0.53)	(± 0.80)	(± 0.36)	(± 0.61)										

*Although FARE achieves the highest clean accuracy, SAFT-L surpasses it by 17.46% and SAFT-M by 15.90% in averaged zero-shot robustness.

strengthen adversarial examples; (iv) PMG-AFT (Wang et al., 2024a), which uses auxiliary branches to align clean and adversarial representations and mitigate overfitting; and (v) TGA-ZSR (Yu et al., 2024), which leverages text-guided attention and achieves SOTA performance on zero-shot robustness benchmarks.

Implementation Details. We adopt TGA-ZSR (Yu et al., 2024) as the default loss function to further push the upper bound of CLIP’s zero-shot accuracy-robustness trade-off by building on its strong foundation. We use refined descriptions with top-5 relevance scores (see Section 5.3). To ensure fair comparison, we follow Yu et al. (2024) in using ViT-B/32 as the backbone and SGD optimizer with a learning rate of 1e-4, momentum 0.9, weight decay 0, and batch size 128. During training, AEs are generated via ℓ_∞ -norm PGD-2 (Madry et al., 2018) with $\epsilon = 1/255$. For evaluation, we use mainly use PGD, AutoAttack (Croce & Hein, 2020), and C&W (Carlini & Wagner, 2017) to evaluate zero-shot robustness. For experiments fine-tuned on Tiny-ImageNet, all models are fine-tuned for 10 epochs. Due to limited computational resources, for experiments fine-tuned on ImageNet-1K, all models are fine-tuned for only 1 epoch.

Hyperparameters for Generating Descriptions. For SAFT-L, we adopt (Pratt et al., 2023), which uses LLMs to generate class-specific textual descriptions. All descriptions are generated by the prompt “*What does a {label} look like*”. These textual descriptions are publicly available at: <https://github.com/sarahpratt/CuPL/tree/main>. For SAFT-M, we adopt (Cai et al., 2025), which propose to capture multiple common and unique features for each class. For each label, we provide 5 images that are randomly sampled from the training data with “*This is a photo of {label}*” and additional prompts “*Describe the unique appearance of a {label} compared to other objects. Use one short sentence*” and “*Describe the appearance of the object {label}. Use one short sentence*”. The MLLM we use is GPT-4o-mini (OpenAI, 2023). We set the temperature to be 0.99, max tokens to be 100 and number of responses for each prompt to be 5.

5.2 Evaluation of Zero-shot Classification

Result Analysis on Tiny-ImageNet. As shown in Table 1, both SAFT-L and SAFT-M significantly improves zero-shot robustness against PGD-100, outperforming the previous SOTA (TGA-ZSR) by 3.85% and 2.28% on average across 15 target datasets and by 5.40% and 2.92% on Tiny-ImageNet, respectively. Notably, SAFT-L consistently performs better across most of the remaining datasets, validating the benefit of semantically enriched text supervision in adversarial fine-tuning. In terms of clean accuracy, SAFT-L and SAFT-M rank second and third overall, achieving 55.27% and 56.01% average clean accuracy, respectively.

Table 2: Robust accuracy (%) of different methods against AutoAttack ($\epsilon = 1/255$) and C&W attack ($\epsilon = 1/255$) across 16 datasets. Tiny-ImageNet is the source dataset and the others are zero-shot datasets. The best accuracy is highlighted in **bold** and the second-best accuracy is underlined.

Method	Source	Datasets for Evaluating Zero-shot Classification Accuracies															Zero-shot Average
		Tiny-ImageNet	CIFAR-10	CIFAR-100	Food101	STL-10	OxfordPets	Flowers102	DTD	EuroSAT	FGVC-Aircraft	Caltech-101	Caltech-256	StanfordCars	PCAM	ImageNet-1K	
AutoAttack ($\epsilon = 1/255$)																	
TeCoA	27.21	29.81	14.23	11.64	66.20	32.46	16.91	13.09	5.77	1.29	51.55	38.58	6.77	32.71	16.21	17.41	23.64
PMG-AFT	29.99	48.66	<u>23.64</u>	14.32	67.59	32.41	13.86	11.65	8.81	0.99	51.26	40.25	9.59	38.53	19.17	<u>19.63</u>	26.69
TGA-ZSR	48.95	40.28	22.33	<u>15.03</u>	<u>71.90</u>	39.49	<u>21.81</u>	<u>16.38</u>	<u>11.27</u>	<u>2.31</u>	<u>57.75</u>	<u>45.41</u>	<u>10.20</u>	<u>40.86</u>	<u>19.20</u>	19.11	<u>28.89</u>
SAFT-L	50.40	<u>42.88</u>	24.54	<u>15.12</u>	73.93	<u>36.11</u>	22.65	17.55	12.91	2.79	59.64	45.64	12.19	43.96	20.22	20.81	30.06
C&W ($\epsilon = 1/255$)																	
TeCoA	28.25	31.11	14.85	12.01	66.65	33.96	17.29	13.09	7.26	1.50	39.34	52.66	7.60	32.06	14.24	15.26	23.93
PMG-AFT	30.30	49.11	<u>23.87</u>	14.36	67.64	32.65	13.90	11.44	8.76	1.05	51.55	33.81	4.69	48.33	12.92	13.33	25.83
TGA-ZSR	<u>44.53</u>	36.42	19.19	<u>19.56</u>	<u>74.00</u>	<u>42.52</u>	<u>22.87</u>	<u>16.49</u>	<u>9.90</u>	<u>2.91</u>	<u>59.88</u>	<u>49.73</u>	<u>12.34</u>	41.48	<u>19.89</u>	<u>21.95</u>	<u>29.94</u>
SAFT-L	58.21	57.73	32.04	30.50	82.19	50.40	31.52	20.96	13.19	3.93	68.23	57.68	17.14	<u>42.93</u>	24.53	28.73	37.45

Table 3: Ablation study on semantic filtering. We report clean and robust accuracy (%) against PGD-100 ($\epsilon = 1/255$) of SAFT-L across 16 datasets. Tiny-ImageNet is the source dataset and the others are zero-shot datasets. The best accuracy is highlighted in **bold**.

Semantic Filtering	Source	Datasets for Evaluating Zero-shot Classification Accuracies															Zero-shot Average	
		Tiny-ImageNet	CIFAR-10	CIFAR-100	Food101	STL-10	OxfordPets	Flowers102	DTD	EuroSAT	FGVC-Aircraft	Caltech-101	Caltech-256	StanfordCars	PCAM	ImageNet-1K		
Robust																		
Robust	<input checked="" type="checkbox"/>	53.15	51.88	27.25	25.26	80.20	44.69	25.87	18.40	10.96	4.02	61.53	51.29	13.09	46.09	20.69	23.36	33.64
	<input checked="" type="checkbox"/>	53.27	52.26	<u>28.34</u>	<u>25.67</u>	<u>78.97</u>	46.07	<u>30.22</u>	<u>20.74</u>	<u>12.42</u>	<u>4.53</u>	<u>64.67</u>	<u>54.27</u>	<u>15.86</u>	<u>47.09</u>	<u>22.74</u>	<u>26.33</u>	<u>35.35</u>
Clean																		
Clean	<input checked="" type="checkbox"/>	73.03	86.52	56.05	59.02	94.04	77.05	45.32	29.40	25.76	12.19	80.72	73.88	32.40	49.73	44.86	50.44	54.49
	<input checked="" type="checkbox"/>	73.47	85.81	57.26	58.69	93.30	<u>77.90</u>	<u>48.96</u>	<u>30.05</u>	<u>25.83</u>	<u>13.39</u>	79.89	<u>74.39</u>	<u>35.18</u>	<u>49.86</u>	<u>46.61</u>	51.91	<u>55.27</u>

Although FARE achieves the highest clean accuracy, SAFT-L surpasses it by 17.46% in average zero-shot robustness, and SAFT-M by 15.90%. These results demonstrate that SAFT-based methods can notably improve the accuracy-robustness trade-off.

Result Analysis on ImageNet-1K. As shown in Table 7, when scaling to ImageNet-1K, SAFT-M exhibits notably improved performance in zero-shot clean accuracy, achieving the highest overall score of 63.69% across 15 target datasets. This demonstrates the scalability of SAFT-based methods under larger-scale pre-training. In terms of robustness, while PMG-AFT achieves the highest zero-shot robust accuracy, it comes at the cost of significantly lower clean accuracy. In contrast, both SAFT-M and SAFT-L attain comparable robustness while outperforming PMG-AFT by 8.70% and 8.15% in clean accuracy, respectively. This clearly highlights the advantage of SAFT-based methods in achieving a more favorable accuracy-robustness trade-off when fine-tuned on large-scale datasets.

5.3 Ablation Studies

Ablation Study on K . We investigate how the number of selected textual descriptions K in Eq. (3) affects the performance of SAFT-L against PGD-100 on four datasets, including one source dataset (i.e., Tiny-ImageNet) and three zero-shot datasets (i.e., CIFAR-10, CIFAR-100 and STL-10) in Appendix A.2. We find that more textual descriptions per class do not necessarily imply better performance. Specifically, when $K = 5$, SAFT-L can achieve the best robustness-accuracy trade-off on average (see Table 8). Therefore, in this paper, we use $K = 5$ for all the experiments.

Ablation Study on Unseen Attacks. We also evaluate transferability to unseen attacks, using AutoAttack and C&W across 16 datasets in Table 2. We compare SAFT-L with the top three baselines on zero-shot

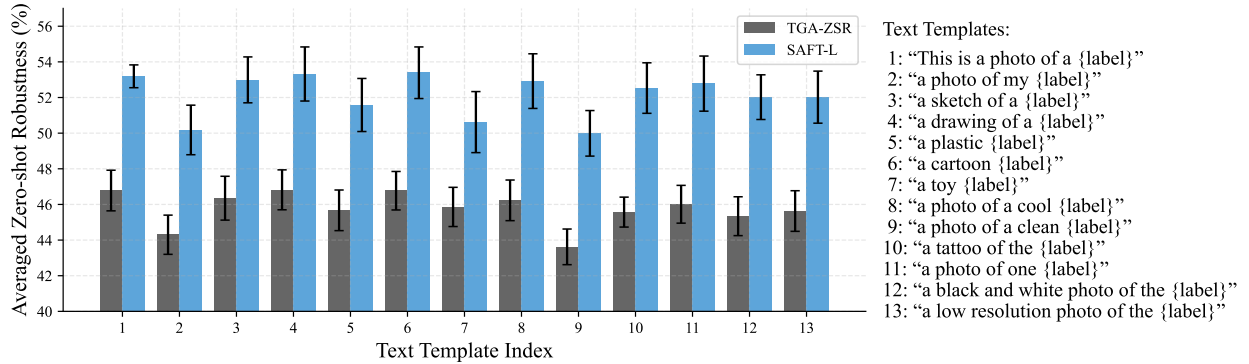


Figure 3: Transferability to different text templates. We compare SAFT-L and TGA-ZSR across 13 text templates, using Tiny-ImageNet as the source dataset and PGD-100 as the evaluation method. We report the standard deviations and averaged zero-shot robustness (%) on CIFAR-10, CIFAR-100, and STL-10 for three runs. SAFT-L *consistently* outperforms TGA-ZSR in averaged zero-shot robust accuracy across all templates. We provide full experimental results in Appendix A.4.

Table 4: Clean and robust accuracy (%) against PGD-100 ($\epsilon = 1/255$) of different methods across 16 datasets using CLIP-L/14. Tiny-ImageNet is the source dataset and the others are zero-shot datasets.

Method	Source	Datasets for Evaluating Zero-shot Classification Accuracies																
		Tiny-ImageNet	CIFAR-10	CIFAR-100	Food101	STL-10	OxfordPets	Flowers102	DTD	EuroSAT	FGVC-Aircraft	Caltech-101	Caltech-256	StanfordCars	PCAM	ImageNet-1K	SUN397	Zero-shot Average
Clean	FARE	68.23	89.19	57.77	72.12	97.01	87.08	63.26	35.80	25.32	20.61	86.71	81.89	56.19	50.89	55.15	49.33	61.89
	SAFT-L	80.39	89.49	61.84	66.24	95.64	86.64	66.24	39.15	32.13	18.06	86.70	82.04	52.03	57.17	57.43	56.02	63.12
Robust	FARE	42.20	45.82	30.73	36.74	80.18	70.73	46.85	24.68	12.07	11.31	75.50	64.35	36.31	49.42	35.09	32.89	43.51
	SAFT-L	68.06	66.60	45.50	51.38	95.64	86.64	66.24	37.00	23.22	16.59	79.07	72.15	43.86	50.52	50.70	50.93	53.52

robustness (i.e., TGA-ZSR, PMG-AFT and TeCoA). Results show that SAFT-L consistently improves zero-shot robust accuracy, achieving average gains of 1.17% on AutoAttack and 7.51% on C&W attack.

Ablation Study on Semantic Filtering. We investigate the effect of semantic filtering in our method by comparing performance with and without this step under PGD-100 attacks in Table 3. Incorporating semantic filtering yields an average improvement of 1.71% in zero-shot robust accuracy. This suggests that the quality of textual descriptions is key to our method.

Ablation Study on LLMs. We conduct an ablation study using Qwen3-4b-instruct (Yang et al., 2025), Qwen3-4b (Yang et al., 2025), Llama-3.2-1b-instruct (Grattafiori et al., 2024) and Llama-3.2-3b-instruct (Grattafiori et al., 2024) to generate descriptions, respectively. Overall, as shown in Appendix A.3, instruction-tuned models with larger size can generate better descriptions. However, we want to highlight that, in our framework, the quality of semantic descriptions is the fundamental factor that drives robustness improvements. LLMs serve as a practical and scalable implementation for generating such descriptions, but they are not an essential component of the method itself. Any mechanism capable of producing semantically accurate and conceptually rich descriptions could, in principle, be used in place of an LLM.

5.4 More Empirical Analysis

Transferability to Different Text Templates. Prior methods use a single template (e.g. “This is a photo of a {label}”) to define class semantics, which limits the robustness to semantic variations. We investigate the transferability of SAFT-L and TGA-ZSR on 13 templates¹, including 1 seen (i.e., “This is a photo of a {label}”) and 12 unseen variants, across 3 target datasets (i.e., CIFAR-10, CIFAR-100, and STL-10). As shown in Figure 3, SAFT-L consistently outperforms TGA-ZSR in averaged zero-shot robust accuracy across

¹Prompt templates are randomly selected from https://github.com/chs20/RobustVLM/blob/main/CLIP_eval/zeroshot-templates.json.

Table 5: Image retrieval recall (IRR) (%) and text retrieval recall (TRR) (%) of different methods on COCO, Flickr8k, and Flickr30k against AutoAttack ($\epsilon = 1/255$).

Method	COCO		Flickr8k		Flickr30k	
	IRR	TRR	IRR	TRR	IRR	TRR
TGA-ZSR	34.27	41.64	57.40	66.80	61.14	69.40
SAFT-L	35.36	43.32	58.86	68.60	63.86	72.10

Table 6: Comparison of training memory usage and training time of different methods.

Methods	GPU	Batch Size	Training Memory Usage	Training Time (Per Epoch / Batch)
TeCoA			13977Mb	801s / 1.03s
PMG-AFT			18423Mb	660s / 0.84s
TGA-ZSR	1 * NVIDIA A100	128	21253Mb	786s / 1.01s
SAFT-L ($K = 5$)			38839Mb	1098s / 1.41s

both seen and unseen templates. We provide full experimental results in Appendix A.4. Specifically, SAFT-L improves averaged zero-shot robust accuracy by 6.41% on the training template and up to 6.96% on unseen variants such as “a tattoo of the {label}”. These results highlight SAFT’s ability to capture semantic diversity beyond fixed linguistic patterns.

Adaptability to Larger Perturbation Budget. We further evaluate our method under a larger perturbation budget in Appendix A.5. This evaluates whether models trained on weaker AEs generalize to stronger attacks. In Table 11, under $\epsilon = 4/255$, SAFT-L still outperforms baseline methods by at least 1.52%.

Scalability to CLIP-L/14. We investigate the scalability of SAFT-L on CLIP-L/14 in Table 4. Notably, when scaled to CLIP-L/14, SAFT-L outperforms FARE by approximately 2% in clean accuracy and 10% in robust accuracy, demonstrating its strong scalability to larger VLMs. This result is particularly surprising, as SAFT-L slightly lagged behind FARE in clean accuracy when using CLIP-B/32, suggesting that larger VLMs better leverage the semantic richness during the fine-tuning.

Applicability to Image-text Retrieval Task. To demonstrate SAFT’s applicability beyond classification, we conduct an additional experiment on the image-text retrieval task in Table 5. Specifically, we replace the original CLIP image encoder with the adversarially fine-tuned image encoder from SAFT-L and TGA-ZSR. We compare the image retrieval recall and text retrieval recall on 3 benchmark image-text retrieval datasets: COCO (Lin et al., 2014), Flickr8k (Hodosh et al., 2013), and Flickr30k (Plummer et al., 2015). Our method consistently outperforms TGA-ZSR by a notable margin.

Generalizability to Out-of-domain Datasets. To evaluate whether the robustness gains of SAFT extend beyond ImageNet-like visual semantics, we further test the models on two genuinely out-of-domain datasets: TU-Berlin sketch dataset (Eitz et al., 2012) and ImageNet-R (Hendrycks et al., 2020). They differ substantially from ImageNet-like natural images. Sketch consists of hand-drawn line sketches without texture or color information, while ImageNet-R contains artistic renditions such as cartoons and paintings that preserve high-level semantics but significantly alter visual appearance. As shown in Appendix A.6, SAFT-L consistently outperforms TGA-ZSR by a notable margin.

5.5 Compute Resources

We compare the memory usage and training time of SAFT-L² with baseline methods in Table 6. Inference time is similar across all methods and thus omitted. Introducing multiple semantic descriptions increases memory and training overhead. For example, SAFT requires 0.4 seconds more per batch than TGA-ZSR. However, given the trade-off between computational cost and the performance of SAFT, it is worthwhile to introduce semantically enriched text during fine-tuning.

²SAFT-M consumes exactly the same memory usage and training time as SAFT-L.

6 Limitations

Dependence on the Quality of Foundation Models. SAFT relies on foundation models to generate semantic descriptions for each class. The effectiveness of this process depends on the relevance, faithfulness, and diversity of the generated descriptions. In cases where the foundation model produces hallucinated or semantically ambiguous prompts, the resulting descriptions may be suboptimal. To mitigate this issue, we propose a *semantic filtering strategy* to filter out descriptions with low relevance scores.

Extra Computational Cost. The integration of an ensemble of textual descriptions will inevitably bring some extra cost. Luckily, we find that this process is lightweight, making SAFT computationally feasible compared to existing adversarial fine-tuning methods.

7 Conclusion

In this paper, we find that AEs generated using cosine similarity may fail to fool CLIP when the similarity metric is replaced with semantically enriched alternatives, making the image encoder fine-tuned with these AEs less robust. To address this problem, we propose *Semantic-aware Adversarial Fine-Tuning* (SAFT), a new framework that generates semantic-aware AEs by incorporating hallucination-aware textual descriptions during the fine-tuning. Extensive experiments show that SAFT notably improves zero-shot adversarial robustness across 16 datasets compared to current SOTA methods and can generalize well to unseen templates. In general, we hope this simple yet effective framework could open up a new perspective in the adversarial fine-tuning of CLIP and lay the groundwork for future methods that account for richer text supervision.

Impact Statement

This study on adversarial fine-tuning for CLIP raises important ethical considerations that we have carefully addressed. We have taken steps to ensure our method is fair. We use widely accepted public benchmark datasets to ensure comparability of our results. Our evaluation encompasses a wide range of attack types and strengths to provide a comprehensive assessment. We have also carefully considered the broader impacts of our work. The proposed adversarial fine-tuning algorithm contributes to the development of more robust machine learning models, potentially improving the reliability of AI systems in various applications. We will actively engage with the community to promote responsible development and use of adversarial fine-tuning.

References

Jean-Baptiste Alayrac, Jeff Donahue, Pauline Luc, Antoine Miech, Iain Barr, Yana Hasson, Karel Lenc, Arthur Mensch, Katherine Millican, Malcolm Reynolds, et al. Flamingo: a visual language model for few-shot learning. *Advances in neural information processing systems*, 35:23716–23736, 2022.

Anish Athalye, Nicholas Carlini, and David Wagner. Obfuscated gradients give a false sense of security: Circumventing defenses to adversarial examples. In *ICML*, 2018.

Anas Awadalla, Irena Gao, Josh Gardner, Jack Hessel, Yusuf Hanafy, Wanrong Zhu, Kalyani Marathe, Yonatan Bitton, Samir Yitzhak Gadre, Shiori Sagawa, Jenia Jitsev, Simon Kornblith, Pang Wei Koh, Gabriel Ilharco, Mitchell Wortsman, and Ludwig Schmidt. Openflamingo: An open-source framework for training large autoregressive vision-language models. *CoRR*, abs/2308.01390, 2023.

Jinze Bai, Shuai Bai, Shusheng Yang, Shijie Wang, Sinan Tan, Peng Wang, Junyang Lin, Chang Zhou, and Jingren Zhou. Qwen-vl: A frontier large vision-language model with versatile abilities. *arXiv preprint arXiv:2308.12966*, 2023.

Lukas Bossard, Matthieu Guillaumin, and Luc Van Gool. Food-101 - mining discriminative components with random forests. In *ECCV*, 2014.

Chengyi Cai, Zesheng Ye, Lei Feng, Jianzhong Qi, and Feng Liu. Attribute-based visual reprogramming for image classification with clip. In *ICLR*, 2025.

Nicholas Carlini and David Wagner. Towards evaluating the robustness of neural networks. In *S&P*, 2017.

Mircea Cimpoi, Subhransu Maji, Iasonas Kokkinos, Sammy Mohamed, and Andrea Vedaldi. Describing textures in the wild. In *CVPR*, 2014.

Adam Coates, Andrew Y. Ng, and Honglak Lee. An analysis of single-layer networks in unsupervised feature learning. In *AISTATS*, 2011.

Francesco Croce and Matthias Hein. Reliable evaluation of adversarial robustness with an ensemble of diverse parameter-free attacks. In *ICML*, 2020.

Francesco Croce, Maksym Andriushchenko, Vikash Sehwag, Edoardo Debenedetti, Nicolas Flammarion, Mung Chiang, Prateek Mittal, and Matthias Hein. Robustbench: a standardized adversarial robustness benchmark. In *NeurIPS*, 2021.

Jia Deng, Wei Dong, Richard Socher, Li-Jia Li, Kai Li, and Li Fei-Fei. Imagenet: A large-scale hierarchical image database. In *CVPR*, 2009.

Mathias Eitz, James Hays, and Marc Alexa. How do humans sketch objects? *ACM Transactions on Graphics*, 31:1 – 10, 2012.

Zhe Gan, Yen-Chun Chen, Linjie Li, Chen Zhu, Yu Cheng, and Jingjing Liu. Large-scale adversarial training for vision-and-language representation learning. In *NeurIPS*, 2020.

Ian J. Goodfellow, Jonathon Shlens, and Christian Szegedy. Explaining and harnessing adversarial examples. In *ICLR*, 2015.

Aaron Grattafiori, Abhimanyu Dubey, Abhinav Jauhri, Abhinav Pandey, Abhishek Kadian, Ahmad Al-Dahle, Aiesha Letman, Akhil Mathur, Alan Schelten, Alex Vaughan, Amy Yang, Angela Fan, Anirudh Goyal, Anthony Hartshorn, Aobo Yang, Archi Mitra, Archie Sravankumar, Artem Korenev, Arthur Hinsvark, Arun Rao, Aston Zhang, Aurelien Rodriguez, Austen Gregerson, Ava Spataru, Baptiste Roziere, Bethany Biron, Binh Tang, Bobbie Chern, Charlotte Caucheteux, Chaya Nayak, Chloe Bi, Chris Marra, Chris McConnell, Christian Keller, Christophe Touret, Chunyang Wu, Corinne Wong, Cristian Canton Ferrer, Cyrus Nikolaidis, Damien Allonsius, Daniel Song, Danielle Pintz, Danny Livshits, Danny Wyatt, David Esiobu, Dhruv Choudhary, Dhruv Mahajan, Diego Garcia-Olano, Diego Perino, Dieuwke Hupkes, Egor Lakomkin, Ehab AlBadawy, Elina Lobanova, Emily Dinan, Eric Michael Smith, Filip Radenovic, Francisco Guzmán, Frank Zhang, Gabriel Synnaeve, Gabrielle Lee, Georgia Lewis Anderson, Govind Thattai, Graeme Nail, Gregoire Mialon, Guan Pang, Guillem Cucurell, Hailey Nguyen, Hannah Korevaar, Hu Xu, Hugo Touvron, Iliyan Zarov, Imanol Arrieta Ibarra, Isabel Kloumann, Ishan Misra, Ivan Evtimov, Jack Zhang, Jade Copet, Jaewon Lee, Jan Geffert, Jana Vranes, Jason Park, Jay Mahadeokar, Jeet Shah, Jelmer van der Linde, Jennifer Billock, Jenny Hong, Jenya Lee, Jeremy Fu, Jianfeng Chi, Jianyu Huang, Jiawen Liu, Jie Wang, Jiecao Yu, Joanna Bitton, Joe Spisak, Jongsoo Park, Joseph Rocca, Joshua Johnstun, Joshua Saxe, Junteng Jia, Kalyan Vasuden Alwala, Karthik Prasad, Kartikeya Upasani, Kate Plawiak, Ke Li, Kenneth Heafield, Kevin Stone, Khalid El-Arini, Krithika Iyer, Kshitiz Malik, Kuenley Chiu, Kunal Bhalla, Kushal Lakhotia, Lauren Rantala-Yearly, Laurens van der Maaten, Lawrence Chen, Liang Tan, Liz Jenkins, Louis Martin, Lovish Madaan, Lubo Malo, Lukas Blecher, Lukas Landzaat, Luke de Oliveira, Madeline Muzzi, Mahesh Pasupuleti, Mannat Singh, Manohar Paluri, Marcin Kardas, Maria Tsimpoukelli, Mathew Oldham, Mathieu Rita, Maya Pavlova, Melanie Kambadur, Mike Lewis, Min Si, Mitesh Kumar Singh, Mona Hassan, Naman Goyal, Narjes Torabi, Nikolay Bashlykov, Nikolay Bogoychev, Niladri Chatterji, Ning Zhang, Olivier Duchenne, Onur Çelebi, Patrick Alrassy, Pengchuan Zhang, Pengwei Li, Petar Vasic, Peter Weng, Prajjwal Bhargava, Pratik Dubal, Praveen Krishnan, Punit Singh Koura, Puxin Xu, Qing He, Qingxiao Dong, Ragavan Srinivasan, Raj Ganapathy, Ramon Calderer, Ricardo Silveira Cabral, Robert Stojnic, Roberta Raileanu, Rohan Maheswari, Rohit Girdhar, Rohit Patel, Romain Sauvestre, Ronnie Polidoro, Roshan Sumbaly, Ross Taylor, Ruan Silva, Rui Hou, Rui Wang, Saghar Hosseini, Sahana Chennabasappa, Sanjay Singh, Sean Bell, Seohyun Sonia Kim, Sergey Edunov, Shaoliang Nie, Sharan Narang, Sharath Raparthy, Sheng Shen, Shengye Wan, Shruti Bhosale, Shun Zhang, Simon Vandenhende, Soumya Batra, Spencer Whitman, Sten Sootla, Stephane Collot, Suchin Gururangan, Sydney Borodinsky, Tamar Herman,

Tara Fowler, Tarek Sheasha, Thomas Georgiou, Thomas Scialom, Tobias Speckbacher, Todor Mihaylov, Tong Xiao, Ujjwal Karn, Vedanuj Goswami, Vibhor Gupta, Vignesh Ramanathan, Viktor Kerkez, Vincent Gonguet, Virginie Do, Vish Vogeti, Vitor Albiero, Vladan Petrovic, Weiwei Chu, Wenhan Xiong, Wenyin Fu, Whitney Meers, Xavier Martinet, Xiaodong Wang, Xiaofang Wang, Xiaoqing Ellen Tan, Xide Xia, Xinfeng Xie, Xuchao Jia, Xuewei Wang, Yaelle Goldschlag, Yashesh Gaur, Yasmine Babaei, Yi Wen, Yiwen Song, Yuchen Zhang, Yue Li, Yuning Mao, Zacharie Delpierre Coudert, Zheng Yan, Zhengxing Chen, Zoe Papakipos, Aaditya Singh, Aayushi Srivastava, Abha Jain, Adam Kelsey, Adam Shajnfeld, Adithya Gangidi, Adolfo Victoria, Ahuva Goldstand, Ajay Menon, Ajay Sharma, Alex Boesenberg, Alexei Baevski, Allie Feinstein, Amanda Kallet, Amit Sangani, Amos Teo, Anam Yunus, Andrei Lupu, Andres Alvarado, Andrew Caples, Andrew Gu, Andrew Ho, Andrew Poulton, Andrew Ryan, Ankit Ramchandani, Annie Dong, Annie Franco, Anuj Goyal, Aparajita Saraf, Arkabandhu Chowdhury, Ashley Gabriel, Ashwin Bharambe, Assaf Eisenman, Azadeh Yazdan, Beau James, Ben Maurer, Benjamin Leonhardi, Bernie Huang, Beth Loyd, Beto De Paola, Bhargavi Paranjape, Bing Liu, Bo Wu, Boyu Ni, Braden Hancock, Bram Wasti, Brandon Spence, Brani Stojkovic, Brian Gamido, Britt Montalvo, Carl Parker, Carly Burton, Catalina Mejia, Ce Liu, Changhan Wang, Changkyu Kim, Chao Zhou, Chester Hu, Ching-Hsiang Chu, Chris Cai, Chris Tindal, Christoph Feichtenhofer, Cynthia Gao, Damon Civin, Dana Beaty, Daniel Kreymer, Daniel Li, David Adkins, David Xu, Davide Testuggine, Delia David, Devi Parikh, Diana Liskovich, Didem Foss, Dingkang Wang, Duc Le, Dustin Holland, Edward Dowling, Eissa Jamil, Elaine Montgomery, Eleonora Presani, Emily Hahn, Emily Wood, Eric-Tuan Le, Erik Brinkman, Esteban Arcaute, Evan Dunbar, Evan Smothers, Fei Sun, Felix Kreuk, Feng Tian, Filippos Kokkinos, Firat Ozgenel, Francesco Caggioni, Frank Kanayet, Frank Seide, Gabriela Medina Florez, Gabriella Schwarz, Gada Badeer, Georgia Swee, Gil Halpern, Grant Herman, Grigory Sizov, Guangyi, Zhang, Guna Lakshminarayanan, Hakan Inan, Hamid Shojanazeri, Han Zou, Hannah Wang, Hanwen Zha, Haroun Habeeb, Harrison Rudolph, Helen Suk, Henry Aspegen, Hunter Goldman, Hongyuan Zhan, Ibrahim Damlaj, Igor Molybog, Igor Tufanov, Ilias Leontiadis, Irina-Elena Veliche, Itai Gat, Jake Weissman, James Geboski, James Kohli, Janice Lam, Japhet Asher, Jean-Baptiste Gaya, Jeff Marcus, Jeff Tang, Jennifer Chan, Jenny Zhen, Jeremy Reizenstein, Jeremy Teboul, Jessica Zhong, Jian Jin, Jingyi Yang, Joe Cummings, Jon Carvill, Jon Shepard, Jonathan McPhie, Jonathan Torres, Josh Ginsburg, Junjie Wang, Kai Wu, Kam Hou U, Karan Saxena, Kartikay Khandelwal, Katayoun Zand, Kathy Matosich, Kaushik Veeraraghavan, Kelly Michelena, Keqian Li, Kiran Jagadeesh, Kun Huang, Kunal Chawla, Kyle Huang, Lailin Chen, Lakshya Garg, Lavender A, Leandro Silva, Lee Bell, Lei Zhang, Liangpeng Guo, Licheng Yu, Liron Moshkovich, Luca Wehrstedt, Madian Khabsa, Manav Avalani, Manish Bhatt, Martynas Mankus, Matan Hasson, Matthew Lennie, Matthias Reso, Maxim Groshev, Maxim Naumov, Maya Lathi, Meghan Keneally, Miao Liu, Michael L. Seltzer, Michal Valko, Michelle Restrepo, Mihir Patel, Mik Vyatskov, Mikayel Samvelyan, Mike Clark, Mike Macey, Mike Wang, Miquel Jubert Hermoso, Mo Metanat, Mohammad Rastegari, Munish Bansal, Nandhini Santhanam, Natascha Parks, Natasha White, Navyata Bawa, Nayan Singhal, Nick Egebo, Nicolas Usunier, Nikhil Mehta, Nikolay Pavlovich Laptev, Ning Dong, Norman Cheng, Oleg Chernoguz, Olivia Hart, Omkar Salpekar, Ozlem Kalinli, Parkin Kent, Parth Parekh, Paul Saab, Pavan Balaji, Pedro Rittner, Philip Bontrager, Pierre Roux, Piotr Dollar, Polina Zvyagina, Prashant Ratanchandani, Pritish Yuvraj, Qian Liang, Rachad Alao, Rachel Rodriguez, Rafi Ayub, Raghotham Murthy, Raghu Nayani, Rahul Mitra, Rangaprabhu Parthasarathy, Raymond Li, Rebekkah Hogan, Robin Battey, Rocky Wang, Russ Howes, Ruty Rinott, Sachin Mehta, Sachin Siby, Sai Jayesh Bondu, Samyak Datta, Sara Chugh, Sara Hunt, Sargun Dhillon, Sasha Sidorov, Satadru Pan, Saurabh Mahajan, Saurabh Verma, Seiji Yamamoto, Sharadh Ramaswamy, Shaun Lindsay, Shaun Lindsay, Sheng Feng, Shenghao Lin, Shengxin Cindy Zha, Shishir Patil, Shiva Shankar, Shuqiang Zhang, Shuqiang Zhang, Sinong Wang, Sneha Agarwal, Soji Sajuyigbe, Soumith Chintala, Stephanie Max, Stephen Chen, Steve Kehoe, Steve Satterfield, Sudarshan Govindaprasad, Sumit Gupta, Summer Deng, Sungmin Cho, Sunny Virk, Suraj Subramanian, Sy Choudhury, Sydney Goldman, Tal Remez, Tamar Glaser, Tamara Best, Thilo Koehler, Thomas Robinson, Tianhe Li, Tianjun Zhang, Tim Matthews, Timothy Chou, Tzook Shaked, Varun Vontimitta, Victoria Ajayi, Victoria Montanez, Vijai Mohan, Vinay Satish Kumar, Vishal Mangla, Vlad Ionescu, Vlad Poenaru, Vlad Tiberiu Mihaiescu, Vladimir Ivanov, Wei Li, Wencheng Wang, Wenwen Jiang, Wes Bouaziz, Will Constable, Xiaocheng Tang, Xiaojian Wu, Xiaolan Wang, Xilun Wu, Xinbo Gao, Yaniv Kleinman, Yanjun Chen, Ye Hu, Ye Jia, Ye Qi, Yenda Li, Yilin Zhang, Ying Zhang, Yossi Adi, Youngjin Nam, Yu, Wang, Yu Zhao, Yuchen Hao, Yundi Qian, Yunlu Li, Yuzi He, Zach Rait, Zachary DeVito, Zef Rosnbrick, Zhaoduo Wen, Zhenyu Yang, Zhiwei

Zhao, and Zhiyu Ma. The llama 3 herd of models, 2024. URL <https://arxiv.org/abs/2407.21783>.

Gregory Griffin, Alex Holub, and Pietro Perona. Caltech-256 object category dataset. 2007.

Patrick Helber, Benjamin Bischke, Andreas Dengel, and Damian Borth. Eurosat: A novel dataset and deep learning benchmark for land use and land cover classification. *IEEE J. Sel. Top. Appl. Earth Obs. Remote. Sens.*, 2019.

Dan Hendrycks, Steven Basart, Norman Mu, Saurav Kadavath, Frank Wang, Evan Dorundo, Rahul Desai, Tyler Lixuan Zhu, Samyak Parajuli, Mike Guo, Dawn Xiaodong Song, Jacob Steinhardt, and Justin Gilmer. The many faces of robustness: A critical analysis of out-of-distribution generalization. *ICCV*, 2020.

Micah Hodosh, Peter Young, and J. Hockenmaier. Framing image description as a ranking task: Data, models and evaluation metrics. *J. Artif. Intell. Res.*, 47:853–899, 2013.

Hanxun Huang, Yisen Wang, Sarah Erfani, Quanquan Gu, James Bailey, and Xingjun Ma. Exploring architectural ingredients of adversarially robust deep neural networks. *NeurIPS*, 2021.

Hanxun Huang, Sarah Monazam Erfani, Yige Li, Xingjun Ma, and James Bailey. X-transfer attacks: Towards super transferable adversarial attacks on CLIP. In *ICML*, 2025.

Andrew Ilyas, Shibani Santurkar, Dimitris Tsipras, Logan Engstrom, Brandon Tran, and Aleksander Madry. Adversarial examples are not bugs, they are features. In *NeurIPS*, 2019.

Jonathan Krause, Michael Stark, Jia Deng, and Li Fei-Fei. 3d object representations for fine-grained categorization. In *ICCV*, 2013.

Alex Krizhevsky, Vinod Nair, and Geoffrey Hinton. CIFAR-10 (canadian institute for advanced research). 2009. URL <http://www.cs.toronto.edu/~kriz/cifar.html>.

Jinhao Li, Haopeng Li, Sarah Erfani, Lei Feng, James Bailey, and Feng Liu. Visual-text cross alignment: Refining the similarity score in vision-language models. *arXiv preprint arXiv:2406.02915*, 2024.

Junnan Li, Dongxu Li, Silvio Savarese, and Steven Hoi. Blip-2: Bootstrapping language-image pre-training with frozen image encoders and large language models. In *International conference on machine learning*, pp. 19730–19742. PMLR, 2023.

Tsung-Yi Lin, Michael Maire, Serge J. Belongie, James Hays, Pietro Perona, Deva Ramanan, Piotr Dollár, and C. Lawrence Zitnick. Microsoft coco: Common objects in context. In *ECCV*, 2014.

Feng Liu, Bo Han, Tongliang Liu, Chen Gong, Gang Niu, Mingyuan Zhou, Masashi Sugiyama, et al. Probabilistic margins for instance reweighting in adversarial training. *NeurIPS*, 2021.

Haotian Liu, Chunyuan Li, Qingyang Wu, and Yong Jae Lee. Visual instruction tuning. In *NeurIPS*, 2023.

Xingjun Ma, Yifeng Gao, Yixu Wang, Ruofan Wang, Xin Wang, Ye Sun, Yifan Ding, Hengyuan Xu, Yunhao Chen, Yunhan Zhao, Hanxun Huang, et al. Safety at scale: A comprehensive survey of large model and agent safety. *Foundations and Trends in Privacy and Security*, 2025.

Aleksander Madry, Aleksandar Makelov, Ludwig Schmidt, Dimitris Tsipras, and Adrian Vladu. Towards deep learning models resistant to adversarial attacks. In *ICLR*, 2018.

Subhransu Maji, Esa Rahtu, Juho Kannala, Matthew B. Blaschko, and Andrea Vedaldi. Fine-grained visual classification of aircraft. *CoRR*, abs/1306.5151, 2013.

Chengzhi Mao, Scott Geng, Junfeng Yang, Xin Wang, and Carl Vondrick. Understanding zero-shot adversarial robustness for large-scale models. In *ICLR*, 2023.

Joshua Maynez, Shashi Narayan, Bernd Bohnet, and Ryan T. McDonald. On faithfulness and factuality in abstractive summarization. In *ACL*, 2020.

Sachit Menon and Carl Vondrick. Visual classification via description from large language models. In *ICLR*, 2023.

Maria-Elena Nilsback and Andrew Zisserman. Automated flower classification over a large number of classes. In *ICVGIP*, 2008.

OpenAI. GPT-4 technical report. *arXiv*, abs/2303.08774, 2023.

Omkar M. Parkhi, Andrea Vedaldi, Andrew Zisserman, and C. V. Jawahar. Cats and dogs. In *CVPR*, 2012.

Bryan A. Plummer, Liwei Wang, Christopher M. Cervantes, Juan C. Caicedo, J. Hockenmaier, and Svetlana Lazebnik. Flickr30k entities: Collecting region-to-phrase correspondences for richer image-to-sentence models. *International Journal of Computer Vision*, 123:74 – 93, 2015.

Sarah M. Pratt, Ian Covert, Rosanne Liu, and Ali Farhadi. What does a platypus look like? generating customized prompts for zero-shot image classification. In *ICCV*, 2023.

Alec Radford, Jong Wook Kim, Chris Hallacy, Aditya Ramesh, Gabriel Goh, Sandhini Agarwal, Girish Sastry, Amanda Askell, Pamela Mishkin, Jack Clark, et al. Learning transferable visual models from natural language supervision. In *ICML*, 2021.

Christian Schlarbmann, Naman Deep Singh, Francesco Croce, and Matthias Hein. Robust clip: Unsupervised adversarial fine-tuning of vision embeddings for robust large vision-language models. In *ICML*, 2024.

Yuhao Sun, Jiacheng Zhang, Zesheng Ye, Chaowei Xiao, and Feng Liu. Sample-specific noise injection for diffusion-based adversarial purification. In *ICML*, 2025.

Yuhao Sun, Chengyi Cai, Jiacheng Zhang, Zesheng Ye, Xingliang Yuan, and Feng Liu. Let's roll a bifta: Bi-refinement for fine-grained text-visual alignment in vision-language models. In *Transactions on Machine Learning Research*, 2026.

Christian Szegedy, Wojciech Zaremba, Ilya Sutskever, Joan Bruna, Dumitru Erhan, Ian J. Goodfellow, and Rob Fergus. Intriguing properties of neural networks. In *ICLR*, 2014.

Shengbang Tong, Ellis L Brown II, Penghao Wu, Sanghyun Woo, ADITHYA JAIRAM IYER, Sai Charitha Akula, Shusheng Yang, Jihan Yang, Manoj Middepogu, Ziteng Wang, et al. Cambrian-1: A fully open, vision-centric exploration of multimodal llms. In *NeurIPS*, 2024.

Dimitris Tsipras, Shibani Santurkar, Logan Engstrom, Alexander Turner, and Aleksander Madry. Robustness may be at odds with accuracy. In *ICLR*, 2019.

Bastiaan S. Veeling, Jasper Linmans, Jim Winkens, Taco Cohen, and Max Welling. Rotation equivariant cnns for digital pathology. In *MICCAI*, 2018.

Sibo Wang, Jie Zhang, Zheng Yuan, and Shiguang Shan. Pre-trained model guided fine-tuning for zero-shot adversarial robustness. In *CVPR*, 2024a.

Weihan Wang, Qingsong Lv, Wenmeng Yu, Wenyi Hong, Ji Qi, Yan Wang, Junhui Ji, Zhuoyi Yang, Lei Zhao, Xixuan Song, et al. Coglm: Visual expert for pretrained language models. *arXiv preprint arXiv:2311.03079*, 2023.

Yisen Wang, Difan Zou, Jinfeng Yi, James Bailey, Xingjun Ma, and Quanquan Gu. Improving adversarial robustness requires revisiting misclassified examples. In *ICLR*, 2020.

Zeyu Wang, Xianhang Li, Hongru Zhu, and Cihang Xie. Revisiting adversarial training at scale. In *CVPR*, 2024b.

Dongxian Wu, Shu-Tao Xia, and Yisen Wang. Adversarial weight perturbation helps robust generalization. *NeurIPS*, 2020.

Jianxiong Xiao, James Hays, Krista A. Ehinger, Aude Oliva, and Antonio Torralba. SUN database: Large-scale scene recognition from abbey to zoo. In *CVPR*, 2010.

An Yang, Anfeng Li, Baosong Yang, Beichen Zhang, Binyuan Hui, Bo Zheng, Bowen Yu, Chang Gao, Chengen Huang, Chenxu Lv, Chujie Zheng, Dayiheng Liu, Fan Zhou, Fei Huang, Feng Hu, Hao Ge, Haoran Wei, Huan Lin, Jialong Tang, Jian Yang, Jianhong Tu, Jianwei Zhang, Jianxin Yang, Jiaxi Yang, Jing Zhou, Jingren Zhou, Junyang Lin, Kai Dang, Keqin Bao, Kexin Yang, Le Yu, Lianghao Deng, Mei Li, Mingfeng Xue, Mingze Li, Pei Zhang, Peng Wang, Qin Zhu, Rui Men, Ruize Gao, Shixuan Liu, Shuang Luo, Tianhao Li, Tianyi Tang, Wenbiao Yin, Xingzhang Ren, Xinyu Wang, Xinyu Zhang, Xuancheng Ren, Yang Fan, Yang Su, Yichang Zhang, Yinger Zhang, Yu Wan, Yuqiong Liu, Zekun Wang, Zeyu Cui, Zhenru Zhang, Zhipeng Zhou, and Zihan Qiu. Qwen3 technical report, 2025. URL <https://arxiv.org/abs/2505.09388>.

Lu Yu, Haiyang Zhang, and Changsheng Xu. Text-guided attention is all you need for zero-shot robustness in vision-language models. In *NeurIPS*, 2024.

Hongyang Zhang, Yaodong Yu, Jiantao Jiao, Eric P. Xing, Laurent El Ghaoui, and Michael I. Jordan. Theoretically principled trade-off between robustness and accuracy. In *ICML*, 2019.

Jiacheng Zhang, Feng Liu, Dawei Zhou, Jingfeng Zhang, and Tongliang Liu. Improving accuracy-robustness trade-off via pixel reweighted adversarial training. In *ICML*, 2024.

Jiacheng Zhang, Benjamin I. P. Rubinstein, Jingfeng Zhang, and Feng Liu. One stone, two birds: Enhancing adversarial defense through the lens of distributional discrepancy. In *ICML*, 2025.

Jingfeng Zhang, Jianing Zhu, Gang Niu, Bo Han, Masashi Sugiyama, and Mohan Kankanhalli. Geometry-aware instance-reweighted adversarial training. In *ICLR*, 2021.

Kaiyang Zhou, Jingkang Yang, Chen Change Loy, and Ziwei Liu. Learning to prompt for vision-language models. *IJCV*, 130(9):2337–2348, 2022.

Wanqi Zhou, Shuanghao Bai, Qibin Zhao, and Badong Chen. Revisiting the adversarial robustness of vision-language models: a multimodal perspective. *arXiv preprint arXiv:2404.19287*, 2024.

Deyao Zhu, Jun Chen, Xiaoqian Shen, Xiang Li, and Mohamed Elhoseiny. MiniGPT-4: Enhancing vision-language understanding with advanced large language models. In *ICLR*, 2024.

A Additional Experiments

A.1 Experiment on ImageNet-1K

Table 7: Clean and robust accuracy (%) against PGD-100 ($\epsilon = 1/255$) of different methods across 16 datasets. ImageNet is the source dataset and the others are zero-shot datasets. The best accuracy is highlighted in **bold** and the second-best accuracy is underlined. “Zero-shot Average” refers to the averaged clean/robust accuracy across 15 zero-shot datasets.

Method	Source		Datasets for Evaluating Zero-shot Classification Accuracies														Zero-shot Average										
	ImageNet-1K		CIFAR-10		CIFAR-100		Food101		STL-10		OxfordPets		Flowers102		DTD		EuroSAT		FGVC-Aircraft		Caltech-101		Caltech-256		StanfordCars		
	Clean	Robust	CIFAR-10	CIFAR-100	Food101	STL-10	OxfordPets	Flowers102	DTD	EuroSAT	FGVC-Aircraft	Caltech-101	Caltech-256	StanfordCars	PCAM	Tiny-ImageNet											
Clean	CLIP	67.41	88.18	<u>62.81</u>	<u>73.79</u>	97.09	<u>84.71</u>	56.24	39.15	40.99	15.81	<u>83.98</u>	83.40	42.81	41.45	<u>66.52</u>	<u>61.16</u>	62.54									
	TeCoA	52.38	72.02	41.27	56.30	92.25	77.21	48.48	33.99	20.07	15.21	82.61	77.56	34.17	43.80	53.52	<u>55.17</u>	53.58									
	FARE	54.90	77.81	52.33	70.16	94.29	84.57	57.55	35.90	21.99	16.02	83.37	78.42	47.33	47.27	55.88	51.52	58.29									
	PMG-AFT	49.39	80.43	49.66	65.73	93.99	75.22	48.30	32.55	23.39	12.06	83.60	74.69	30.31	<u>48.21</u>	56.24	50.44	54.99									
	TGA-ZSR	63.44	88.25	57.65	73.94	95.33	84.06	60.43	38.03	<u>39.54</u>	19.08	81.66	81.73	45.73	46.34	64.45	60.23	62.43									
	SAFT-L	63.37	<u>88.33</u>	60.52	74.33	<u>95.94</u>	85.47	61.29	<u>40.21</u>	34.93	<u>17.85</u>	82.95	<u>82.79</u>	<u>46.50</u>	47.29	65.75	62.92	<u>63.14</u>									
Robust	SAFT-M	64.04	89.13	63.03	70.66	95.83	83.57	58.95	40.85	36.35	17.19	85.01	82.40	45.00	57.86	69.22	60.29	63.69									
	CLIP	3.78	7.62	2.94	3.45	33.46	12.02	0.89	2.18	0.04	0.06	30.66	21.58	0.20	0.49	5.05	1.16	7.85									
	TeCoA	28.55	33.01	17.38	25.19	70.35	49.88	27.76	22.66	12.23	5.22	67.70	57.18	11.29	21.41	21.94	28.91	31.29									
	FARE	25.97	37.13	19.37	<u>25.56</u>	72.85	52.85	27.73	20.96	11.39	3.90	63.02	53.00	<u>14.04</u>	24.74	20.05	21.27	30.86									
	PMG-AFT	29.88	40.64	<u>17.77</u>	24.44	81.08	51.16	27.83	23.51	14.41	4.62	69.07	57.22	10.28	<u>23.27</u>	22.16	27.12	32.78									
	TGA-ZSR	30.30	26.18	12.41	24.41	71.86	52.41	27.19	20.74	7.36	4.62	67.36	55.37	12.35	13.16	15.12	22.40	28.95									
SAFT-L	30.82	28.41	13.56	26.19	<u>73.76</u>	56.12	29.84	22.55	<u>12.76</u>	3.75	<u>69.67</u>	<u>57.70</u>	13.47	11.17	18.37	24.97	30.82										
	SAFT-M	32.42	30.36	16.22	24.13	71.53	<u>53.53</u>	26.43	21.91	12.05	<u>4.99</u>	69.97	59.92	<u>14.31</u>	21.84	22.66	25.23	<u>31.67</u>									

A.2 Ablation Study on Number of Descriptions

Table 8: Ablation study on number of descriptions per class. We use M to represent the number of descriptions selected for each class. Tiny-ImageNet is the source dataset and CIFAR-10, CIFAR-100, and STL-10 are zero-shot datasets. The best accuracy is highlighted in **bold** and the second-best accuracy is underlined. We report the averaged results of three runs.

No. of Descriptions	Source		Datasets for Evaluating Zero-shot Classification Accuracies														Average							
	Tiny-ImageNet		CIFAR-10		CIFAR-100		STL-10		CIFAR-10				CIFAR-100				STL-10		CIFAR-10		CIFAR-100		STL-10	
	Clean	Robust	Clean	Robust	Clean	Robust	Clean	Robust	Clean	Robust	Clean	Robust	Clean	Robust	Clean	Robust	Clean	Robust	Clean	Robust	Clean	Robust		
$K = 1$	72.00	49.70	84.92	47.89	56.26	25.77	93.34	77.68	76.63	50.26														
$K = 2$	73.18	<u>50.21</u>	84.85	<u>49.10</u>	56.29	<u>26.10</u>	92.85	77.65	76.80	50.77														
$K = 3$	73.17	43.04	84.86	39.21	56.66	19.18	92.83	74.05	76.88	43.87														
$K = 4$	73.34	44.08	85.11	42.24	56.98	20.95	92.73	74.15	77.04	45.35														
$K = 5$	73.47	53.27	85.81	52.26	57.26	28.34	93.30	78.97	<u>77.46</u>	53.21														
$K = 6$	73.83	48.00	85.38	45.42	57.05	23.48	<u>93.53</u>	77.58	77.45	48.62														
$K = 7$	73.51	44.11	84.86	41.27	<u>57.77</u>	19.37	93.21	75.90	77.34	45.16														
$K = 8$	73.17	47.90	85.22	45.55	57.39	22.49	92.81	76.63	77.15	48.14														
$K = 9$	73.41	45.33	85.15	43.66	57.60	21.15	93.50	75.74	77.41	46.47														
$K = 10$	<u>73.66</u>	43.86	<u>85.41</u>	41.30	58.52	20.63	93.56	74.67	77.79	45.11														

A.3 Ablation Study on LLMs

Table 9: Ablation study on LLMs of varying quality and scale. We report the best in **bold**.

	LLM	Source	Zero-shot Datasets			
			Tiny-ImageNet	CIFAR-10	CIFAR-100	
Clean	Qwen3-4B-instruct	73.96		85.45	55.46	93.58
	Qwen3-4B	73.22		86.35	56.98	93.73
	Llama-3.2-1B-instruct	74.00		86.39	56.42	93.43
	Llama-3.2-3B-instruct	74.05		86.25	56.28	92.31
Robust	Qwen3-4B-instruct	53.45		51.91	27.79	78.91
	Qwen3-4B	47.10		44.96	23.40	76.08
	Llama-3.2-1B-instruct	49.08		46.15	23.98	77.14
	Llama-3.2-3B-instruct	50.14		48.34	26.40	78.34

A.4 Transferability to Different Text Templates

Table 10: Ablation study on text templates. We compare clean and robust accuracy (%) against PGD-100 ($\epsilon = 1/255$) between TGA-ZSR and our method across 4 datasets. Tiny-ImageNet is the source dataset and the others are zero-shot datasets. 13 different text templates are used for evaluation, which include 1 seen template (“This is a photo of a {label}”) and 12 unseen templates. The best accuracy is highlighted in **bold**. The performance improvements and degradation are reported in **green** and **red**, respectively. We report the averaged results of three runs.

Type	Template	Method	Source		Datasets for Evaluating Zero-shot Classification Accuracies						Zero-shot Average		
			Tiny-ImageNet		CIFAR-10		CIFAR-100		STL-10				
			Clean	Robust	Clean	Robust	Clean	Robust	Clean	Robust	Clean	Robust	
Seen	“This is a photo of a {label}”	TGA-ZSR	76.84	47.87	85.90	42.61	57.20	22.27	92.92	75.47	78.67	78.79	53.19 (+6.41)
		SAFT-L	73.47	53.27	85.81	52.26	57.26	28.34	93.30	78.97	78.79 (+0.12)	53.19 (+6.41)	
	“a photo of my {label}”	TGA-ZSR	72.68	43.94	80.61	39.61	50.97	20.18	90.52	73.12	74.03	74.03	44.30
		SAFT-L	70.57	50.71	82.51	48.79	51.77	25.69	91.35	76.07	75.21 (+1.18)	50.18 (+5.88)	
	“a sketch of a {label}”	TGA-ZSR	74.00	45.12	84.41	41.41	55.00	21.64	93.68	76.01	77.69	77.69	46.35
		SAFT-L	71.97	51.73	84.71	51.34	55.41	27.58	94.12	80.05	78.08 (+0.39)	52.99 (+6.64)	
	“a drawing of a {label}”	TGA-ZSR	74.42	45.55	84.86	42.17	55.89	22.24	93.44	76.05	78.06	78.06	46.82
		SAFT-L	72.22	52.05	85.13	52.01	55.67	27.75	94.13	80.19	78.31 (+0.25)	53.32 (+6.50)	
	“a plastic {label}”	TGA-ZSR	71.52	43.58	84.44	41.59	53.72	20.56	92.48	74.87	76.88	76.88	45.67
		SAFT-L	69.50	49.93	83.12	50.00	53.22	26.41	92.69	78.32	76.35 (-0.54)	51.58 (+5.91)	
	“a cartoon {label}”	TGA-ZSR	72.10	43.64	85.55	43.23	53.61	21.57	92.84	75.52	77.33	77.33	46.77
		SAFT-L	71.33	51.09	85.93	53.36	53.95	27.35	93.09	79.45	77.66 (+0.33)	53.39 (+6.62)	
	“a toy {label}”	TGA-ZSR	70.56	42.51	84.58	44.45	51.93	20.50	90.54	72.63	75.68	75.68	45.86
		SAFT-L	69.47	49.59	82.53	50.32	52.48	26.05	89.89	75.49	74.96 (-0.72)	50.62 (+4.76)	
	“a photo of a cool {label}”	TGA-ZSR	75.98	46.76	84.95	41.28	57.02	22.06	92.80	75.34	78.26	78.26	46.23
Unseen	“a photo of a clean {label}”	TGA-ZSR	74.01	45.76	81.67	39.34	54.58	20.85	88.28	70.66	74.85	74.85	43.62
		SAFT-L	71.87	51.70	83.03	49.20	55.43	26.92	89.57	73.86	76.01 (+1.16)	49.99 (+6.37)	
	“a tattoo of the {label}”	TGA-ZSR	69.23	41.47	83.58	41.65	51.53	20.30	92.29	74.76	75.80	75.80	45.57
		SAFT-L	67.44	48.27	83.23	50.91	52.74	26.91	93.63	79.76	76.53 (+0.73)	52.53 (+6.96)	
	“a photo of one {label}”	TGA-ZSR	76.20	46.81	84.87	41.59	56.11	21.20	92.96	75.23	77.98	77.98	46.01
		SAFT-L	73.49	52.85	85.16	51.87	56.50	27.38	93.54	79.08	78.40 (+0.42)	52.78 (+6.77)	
	“a black and white photo of the {label}”	TGA-ZSR	72.11	43.82	84.81	40.71	54.42	20.92	92.45	74.38	77.22	77.22	45.34
		SAFT-L	71.02	50.76	85.59	49.98	55.22	26.75	93.72	79.33	78.17 (+0.95)	52.02 (+6.68)	
	“a low resolution photo of the {label}”	TGA-ZSR	73.85	44.24	85.14	40.44	55.62	21.45	92.44	75.01	77.73	77.73	45.63
		SAFT-L	72.23	51.51	84.71	50.09	55.66	27.02	93.30	78.95	77.89 (+0.16)	52.02 (+6.39)	

A.5 Adaptability to Larger Perturbation Budget

Table 11: Robust accuracy (%) of different methods against PGD-100 ($\epsilon = 4/255$) across 16 datasets. Tiny-ImageNet is the source dataset and the others are zero-shot datasets. The best accuracy is highlighted in **bold** and the second-best accuracy is underlined. “Zero-shot Average” refers to the averaged robust accuracy across 15 zero-shot datasets.

Method	Source	Zero-shot Datasets															
		Tiny-ImageNet	CIFAR-10	CIFAR-100	Food101	STL-10	OxfordPets	Flowers102	DTD	EuroSAT	FGVC-Aircraft	Caltech-101	Caltech-256	StanfordCars	PCAM	ImageNet-1K	SUN397
TeCoA	1.63	0.29	0.45	0.25	9.29	1.25	0.50	<u>2.23</u>	0.00	0.00	11.18	5.80	0.04	<u>2.53</u>	0.58	0.26	2.31
PMG-AFT	4.94	3.77	3.50	1.38	19.54	2.73	<u>2.85</u>	<u>3.99</u>	<u>0.47</u>	<u>0.06</u>	20.33	10.00	<u>0.29</u>	24.33	<u>2.38</u>	<u>1.51</u>	6.47
TGA-ZSR	16.76	<u>12.04</u>	<u>5.04</u>	2.13	<u>36.48</u>	<u>6.80</u>	<u>1.94</u>	0.90	0.00	0.00	<u>22.73</u>	<u>15.05</u>	<u>0.16</u>	0.02	2.51	<u>1.10</u>	<u>7.13</u>
SAFT-L	<u>15.92</u>	19.09	6.87	<u>1.70</u>	43.40	7.20	1.14	0.59	0.00	0.00	27.63	19.15	0.10	0.01	2.11	0.78	8.65

A.6 Generalizability to Out-of-domain Datasets

Table 12: Experiments on TU-Berlin sketch dataset and ImageNet-R. We report the best in **bold**.

	Method	Sketch	ImageNet-R
Clean	TGA-ZSR	36.80	46.74
	SAFT-L	43.85	52.85
Robust	TGA-ZSR	27.05	26.54
	SAFT-L	29.75	29.70